OXFORD

Cerebral Cortex, April 2016;26: 1558–1568

doi: 10.1093/cercor/bhu320
Advance Access Publication Date: 16 January 2015
Original Article

ORIGINAL ARTICLE

Functional Imaging of the Developing Brain at the Bedside Using Diffuse Optical Tomography

Silvina L. Ferradal[1,2], Steve M. Liao[3], Adam T. Eggebrecht[2], Joshua S. Shimony[2], Terrie E. Inder[5], Joseph P. Culver[1,2], and Christopher D. Smyser[3,4]

[1]Department of Biomedical Engineering, Washington University, St Louis, MO, USA, [2]Mallinckrodt Institute of Radiology, [3]Department of Pediatrics, [4]Department of Neurology, Washington University School of Medicine, St Louis, MO, USA, and [5]Department of Pediatric Newborn Medicine, Brigham and Women's Hospital, Boston, MA, USA

Address correspondence to Christopher D. Smyser, Department of Neurology, Division of Pediatric Neurology, Washington University, 660 South Euclid Avenue, Campus Box 8111, St Louis, MO 63110-1093, USA. Email: smyserc@neuro.wustl.edu

Abstract

While histological studies and conventional magnetic resonance imaging (MRI) investigations have elucidated the trajectory of structural changes in the developing brain, less is known regarding early functional cerebral development. Recent investigations have demonstrated that resting-state functional connectivity MRI (fcMRI) can identify networks of functional cerebral connections in infants. However, technical and logistical challenges frequently limit the ability to perform MRI scans early or repeatedly in neonates, particularly in those at greatest risk for adverse neurodevelopmental outcomes. High-density diffuse optical tomography (HD-DOT), a portable imaging modality, potentially enables early continuous and quantitative monitoring of brain function in infants. We introduce an HD-DOT imaging system that combines advancements in cap design, ergonomics, and data analysis methods to allow bedside mapping of functional brain development in infants. In a cohort of healthy, full-term neonates scanned within the first days of life, HD-DOT results demonstrate strong congruence with those obtained using co-registered, subject-matched fcMRI and reflect patterns of typical brain development. These findings represent a transformative advance in functional neuroimaging in infants, and introduce HD-DOT as a powerful and practical method for quantitative mapping of early functional brain development in normal and high-risk neonates.

Key words: developmental neuroimaging, diffuse optical tomography, functional magnetic resonance imaging, infant, neurodevelopment

Introduction

Cerebral structure and function change continuously during early brain development (Tau and Peterson 2010). While histological studies and conventional magnetic resonance imaging (MRI) techniques have elucidated the trajectory of early structural changes in the developing brain (Hill et al. 2010; Jernigan et al. 2011; Dubois et al. 2014), much less is known about early functional cerebral development. Recent investigations have demonstrated that resting-state functional connectivity MRI (fcMRI), which investigates the temporal correlations in low-frequency (<0.1 Hz) fluctuations in blood oxygen level-dependent (BOLD) signal, is a technique well suited to investigations of infants. This modality has been used to identify immature forms of networks of functional cerebral connections that reflect known spatial and functional gradients of cortical gray and white matter development (Fransson et al. 2007; Doria et al. 2010; Smyser et al. 2010). However, substantive technical and logistical challenges frequently limit the ability to perform fcMRI scans readily and longitudinally in infants, particularly in populations at greatest risk for adverse neurodevelopmental outcomes (Glass et al. 2010). Novel approaches that enable early and continuous

assessment of cerebral function may help to improve our understanding of the processes underlying normal and aberrant neurodevelopment and provide opportunities for improvement in clinical care.

Bedside optical imaging systems based on near-infrared spectroscopy (NIRS) principles can provide continuous longitudinal measures of brain function. These systems are well suited for neonatal populations not only because near-infrared light penetrates to deeper brain regions in smaller heads with thinner skulls, but also because this technology is quiet, portable, and potentially less vulnerable to motion artifacts. The vast majority of pediatric optical systems employ sparse arrays of optical probes. This approach, however, suffers from poor image quality, low resolution, and physiological noise contamination that affect the overall reliability. Recent advances in the application of high-density diffuse optical tomography (HD-DOT) in adults have addressed these limitations with dense overlapping measurements, providing improved spatial resolution and better separation of cerebral signals from superficial confounds (Boas et al. 2004; Zeff et al. 2007; Eggebrecht et al. 2012, 2014; Habermehl et al. 2012).

As optical methods can measure similar hemodynamic contrasts to fMRI-BOLD signals, the extension of functional connectivity techniques to HD-DOT maps is relatively direct. However, translation of HD-DOT techniques to neonates involves additional challenges such as cap ergonomics that maximize comfort while improving coupling between the optical probes and the infant's scalp and neonatal head modeling that provides accurate tomographic reconstruction and anatomical registration. Here, we introduce a portable HD-DOT imaging system that combines extended field of view, ergonomics, and realistic head modeling to enable mapping of functional connectivity resting-state networks (RSNs) of the newborn brain at the bedside within the first days of life.

The initial step to successfully establishing functional connectivity HD-DOT (fcDOT) as a tool for assessment of neonatal brain function is to define normal fcDOT patterns in healthy, term-born infants and to perform quantitative voxel-by-voxel validation against the gold standard of fcMRI. By using light propagation models derived from subject-specific structural MRIs, we generated DOT maps that are coregistered to the individual MRI space to allow cross-modality comparisons with fcMRI results at the single-subject and group levels. The strong spatial agreement between results obtained with each approach demonstrates the improved accuracy, spatial localization, and resolution afforded by fcDOT in comparison with existing optical imaging techniques. These findings represent a critical step toward establishing DOT as a clinical tool that allows accurate and reliable continuous longitudinal investigation of cerebral function at the bedside in normal and high-risk neonates.

Materials and Methods

Subjects

Fourteen healthy, full-term infants (gestational age at birth: 37–41 weeks) were recruited from the Newborn Nursery at Barnes-Jewish Hospital in St Louis, Missouri, within the first 48 h of life. Parental informed consent was obtained for each subject prior to participation in the study. All aspects of the study were approved by the Human Research Protection Office of Washington University in St Louis. All infants had no history of in utero illicit substance exposure and no evidence of acidosis (pH <7.20) on umbilical cord or arterial blood gas assessments during the first hour of life. Infants were excluded if found to have chromosomal abnormality or suspected or proven congenital infection (e.g., HIV, sepsis, toxoplasmosis, rubella, cytomegalovirus, and herpes simplex virus). The mean gestational age at birth for the cohort was 39.2 weeks. Demographic information for the cohort is provided in Table 1. Five subjects were excluded due to excessive motion during data acquisition: 3 infants during the DOT scan and 2 infants during the MRI scan.

DOT investigation was performed within the first 24–48 h of life. Nonconcurrent MRI was performed within 1 day of the DOT data acquisition. Infants were studied during natural sleep or while resting quietly without sedating medications for both studies (Mathur et al. 2008).

HD-DOT Data Acquisition

High-Density DOT System

DOT data acquisition was performed using a continuous-wave high-density DOT system with an optode array consisting of 32 sources and 34 detectors. Each source position consisted of light-emitting diodes flashing at 2 near-infrared wavelengths (750 and 850 nm). Source-detector (SD) pair measurements at multiple distances (namely, first through fourth nearest neighbors at 1.0, 2.2,

Table 1 Demographic information for subjects

Subject	Sex	Birthweight (g)	OFC (cm)	GA at birth (weeks)	PMA at DOT (weeks)	PMA at MRI (weeks)	Comments
1	F	2915	33.0	39	39 2/7	39 4/7	fMRI data did not pass noise threshold
2	F	3550	33.5	39	39 2/7	39 3/7	DOT data did not pass noise threshold
3	F	3420	33.0	39	39 2/7	39 3/7	DOT data did not pass noise threshold
4	F	2725	33.5	38	38 3/7	38 5/7	–
5	F	2670	33.0	39	39 2/7	39 3/7	–
6	F	2970	32.5	39	39 2/7	39 3/7	–
7	M	3316	34.5	37	37 2/7	37 3/7	fMRI data did not pass noise threshold
8	M	3230	36.0	39	39 2/7	39 3/7	–
9	M	3725	36.0	41	41 2/7	41 3/7	–
10	F	3215	34.5	41	41 2/7	41 3/7	–
11	M	2965	33.5	39	39 2/7	39 3/7	–
12	M	3140	34.0	40	40 2/7	40 3/7	–
13	F	3005	33.5	38	38 2/7	–	DOT data did not pass noise threshold
14	M	3350	35.5	41	41 2/7	41 3/7	–

F, female; M, male; OFC, occipitofrontal circumference; GA, gestational age; PMA, postmenstrual age.

3.0, and 3.6 cm, respectively) were sampled simultaneously at a frame rate of 10 Hz.

The design of the DOT imaging cap focused on providing stability for efficient optical coupling and optimizing ergonomic comfort for prolonged scanning sessions. During a scanning session, the imaging cap was placed above the inion and extended laterally above the subject's ears (Fig. 1*a*). Based on the current optode arrangement and ergonomic design, cap coverage included the occipital, temporal, and inferior parietal cortices of the infant's head. The structural support of the cap was provided by a layer of flexible plastic molded to fit the curvature of the infant's head. To enhance versatility with different head shapes and sizes, the imaging cap was divided into 5 triangular patches (Fig. 1*b*). All patches were held together by a neoprene headband which was attached to the head with Velcro straps. Flexible optical fiber bundles were embedded in a soft silicone array to provide additional support and prevent skin laceration (Fig. 1*c*). A set of fiducial points (including nasion, inion, pre-auricular points, and the outer lower corners of the optode array) were measured at the end of the scanning session to determine the location of the array relative to the head.

All scans were performed within 1 h after feeding in an isolated, dimly lit room in the nursery. Total duration of the data acquisition ranged from 20 to 60 min depending on each infant's tolerance of scanning.

HD-DOT Data Quality Assessment

Acquiring quality data required in situ optimization of cap fit. To evaluate raw data quality, we developed real-time and off-line visualizations of measurement quality. Average light levels for each SD pair measurement were displayed on an unwrapped and flattened view of the cap (Fig. 1*d*). A satisfactory cap fit exhibited a homogenous distribution of light levels across the entire cap. Noise levels across channels were displayed on a flattened view of the cap (Fig. 1*e*). Measurements exhibiting a variance lower than the noise threshold (channels with standard deviation <7.5% of the mean signal) were shown as green lines between optodes. The temporal mean of SD pair measurements across the cap had a light level fall-off that was logarithmically related to the SD pair separation distance (Fig. 1*f*). Off-line visualizations provided a broader assessment of data quality and aided in the selection of noisy segments during data preprocessing. After cropping the noisy segments, most measurements exhibited a variance lower than the noise threshold (Fig. 1*g*). Power spectra for second nearest-neighbor measurements at both wavelengths showed a clear peak at the pulse frequency as well as strong power in the functional connectivity frequency band (Fig. 1*h*).

MRI Data Acquisition

MRI scans were performed on the second or third day after birth, following the DOT scan. MR imaging was performed on a Siemens Magnetom Trio 3T scanner. Each infant was accompanied to the MRI scanner by a research nurse. Pulse oximetry was used to monitor heart rate and oxygenation throughout the study. Structural and functional images were acquired using the following sequences: (1) T_1-weighted, magnetization-prepared rapid gradient echo [MP-RAGE; time repetition (TR)/time echo (TE) 1550/3.05 ms, voxel size $1.0 \times 1.0 \times 1.3$ mm^3], (2) T_2-weighted, turbo spin echo (TR/TE 8210/161 ms, voxel size $1.0 \times 1.0 \times 1.0$ mm^3), (3) T_2*-weighted, gradient echo planar imaging (EPI) (TR/TE 2910/28 ms, voxel size $2.4 \times 2.4 \times 2.4$ mm^3), and (4) gradient echo field map (TR/TE 400/7.65 ms, voxel size $2.4 \times 2.4 \times 2.4$ mm^3). A total of 250 frames were collected for each resting-state functional sequence (T_2*-weighted gradient EPI). Total scan time for acquisition of all sequences was approximately 50 min.

HD-DOT Data Analysis

Neonatal Head Modeling

To complement the improvements in instrumentation and data quality assessment, a processing pipeline for modeling light propagation in neonatal heads was developed (Supplementary Fig. 1). Subject-specific head models were created using T_1- and T_2-weighted images (Fig. 2*a*). Automatic brain extraction and segmentation were performed using the ANTs software (Avants et al. 2011). The brain segmentation pipeline combines a multivariate expectation–maximization algorithm and a prior based on a T_2-weighted neonatal template composed of 20 subjects. A mask corresponding to extracerebral tissue was extracted from the T_1-weighted images using thresholding and morphological operations. Owing to the poor contrast of neonatal MR images with respect to bone, the extracerebral tissue mask combined scalp and skull tissue (Fig. 2*b*). A finite element model (FEM) was created from the segmented images using the Nirview software (Jermyn et al. 2013) (Fig. 2*c*). The imaging array was mapped onto the FEM using the anatomical measurements obtained during the DOT scanning session (Fig. 2*d*). Optical properties were assigned to each node according to the tissue type determined by the segmentation mask (see Supplementary Table 1). A subject-specific sensitivity matrix was obtained using the Nirfast light modeling software (Dehghani et al. 2008; Fig. 2*e*). Note that the sensitivity profile decays as a function of depth, limiting the effective penetration to approximately 2 cm below the head surface.

HD-DOT Data Preprocessing and Reconstruction

Visible noisy segments were cropped manually from each SD pair measurement aided by off-line visualizations of SD pair measurement time traces (as described in the "HD-DOT Data Quality Assessment" subsection). Log-ratio data were bandpass filtered to 0.009–0.08 Hz. Superficial and systemic hemodynamic artifacts were regressed. Only first and second nearest-neighbor measurements that passed the noise threshold (i.e., measurements that exhibited a standard deviation <7.5% of the mean signal) were used for the image reconstruction. A minimum of 5 min of low motion data were required for each subject. Subjects that did not meet these criteria were excluded due to excessive motion. The average length of the DOT time series included in the analysis was 7.2 min.

Volumetric reconstructions of absorption coefficients at both 750 and 850 nm were obtained using the inverted sensitivity matrix computed for each subject. Three-dimensional maps of concentration changes of oxyhemoglobin (ΔHbO_2) and deoxyhemoglobin (ΔHbR) were computed using the extinction coefficients of each hemoglobin species (Wray et al. 1988).

fcMRI Data Analysis

fcMRI Data Preprocessing

Standard preprocessing of the BOLD data was performed to exclude signal change caused by non-neuronal causes and to correct for head motion [for further details, see Smyser et al. (2010)]. T_2-weighted images were aligned with a full-term neonatal target and the first BOLD frame was coregistered to the corrected T_2-weighted image. Field map correction was then applied

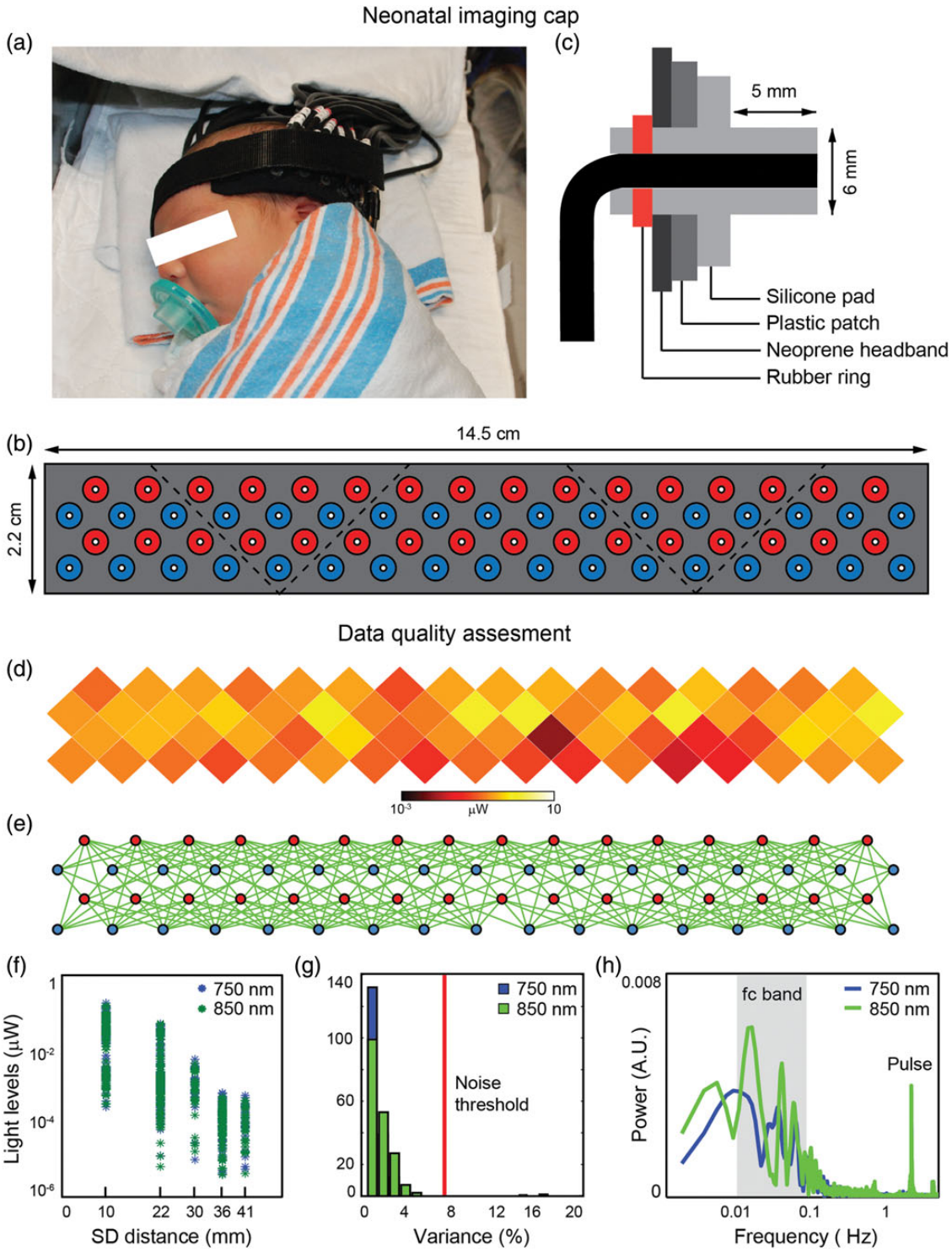

Figure 1. DOT data acquisition. Neonatal imaging cap: The neonatal imaging cap was designed to provide comfort while maximizing coupling between the optodes and the infant's scalp. (*a*) During a scanning session, the cap was placed on the back of the head, above the inion, and extended laterally above the infant's ears. (*b*) To improve ergonomics, the cap was divided into 5 patches of flexible plastic molded to fit the infant's head curvature. All patches were attached to a neoprene headband that is wrapped around the infant's head using Velcro straps. (*c*) Silicone nubs (6 mm diameter) were attached to the fiberoptic tips through rubber rings to avoid scratches and increase comfort. Data quality assessment: (*d*) Average light levels for each optode position were displayed on an unwrapped and flattened view of the cap. (*e*) Measurements that passed the noise threshold were shown as green lines between optodes. (*f*) The temporal mean of measurements across the cap had a light level fall-off that was logarithmically related to the SD pair separation distance. (*g*) After cropping the noisy segments, most measurements exhibited a variance lower than the noise threshold (7.5%). (*h*) Power spectra for second nearest-neighbor measurements at both wavelengths showed a clear peak at the pulse frequency (~2.2 Hz) as well as strong power in the functional connectivity frequency band (0.009–0.08 Hz).

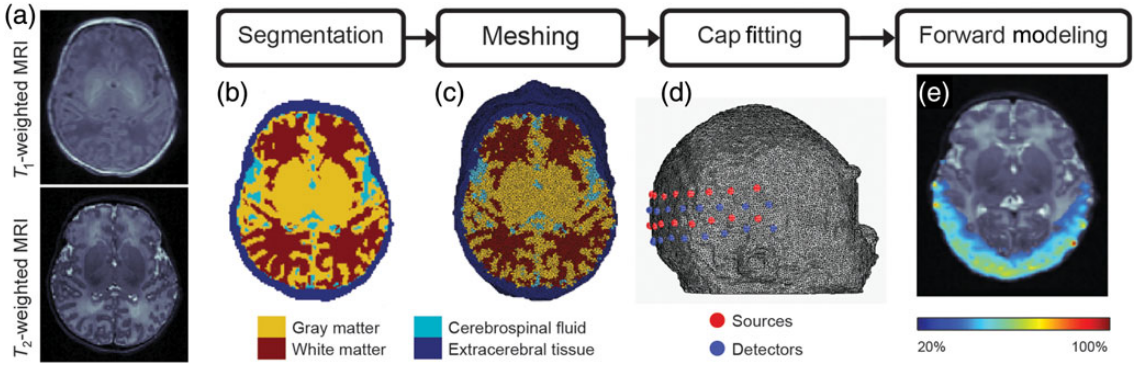

Figure 2. Neonatal head modeling. (*a*) Anatomical MR images (T_1-weighted and T_2-weighted) obtained for each individual infant were used to create a subject-specific head model. (*b*) The MR images were first segmented into 4 tissue types, namely, gray matter (GM), white matter (WM), CSF, and extracerebral tissue (scalp and skull). (*c*) A FEM was created using the Nirview modeling software and then optical properties were assigned to each node according to the tissue type determined by the segmentation. (*d*) The optode grid was placed over the head model based on the fiducial points measured during the DOT scanning session. (*e*) A subject-specific sensitivity matrix was calculated using the NIRFAST light modeling software.

to compensate for spatial distortions caused by magnetic field inhomogeneities. Temporal bandpass filtering from 0.009 to 0.08 Hz was applied to the BOLD data. Linear regression was performed using the following nuisance regressors: (1) Global brain signal averaged over the brain region in the atlas space, (2) motion estimates (including translations, rotations, and derivatives in the 3 orthogonal directions), and (3) white matter and cerebrospinal fluid (CSF) regressors (computed as an average of multiple regions of interest (ROIs) identified in the coregistered T_2-weighted images). Frames corrupted by motion were excluded from further analysis using an established motion detection strategy (Power et al. 2012) and stringent data quality criteria [i.e., frames with framewise displacement >1 mm and root-mean-squared BOLD signal intensity change (DVARS) >1% were removed from the fMRI time series]. A minimum of 5 min of usable fMRI data were required for inclusion in subsequent analyses. Subjects that did not meet these criteria were excluded due to excessive motion. The average number of frames used across subjects after motion detection was 143 (~7 min).

fcDOT and fcMRI Functional Connectivity Analyses

Spatial Smoothing and Normalization

DOT data have a spatial resolution of approximately 10 mm, whereas the fMRI data have a slightly higher resolution (~6 mm in 3T scanners). Prior to correlation analysis, both data sets were spatially smoothed using a smoothing kernel that matches the spatial resolution of each modality [i.e., full-width-at-half-maximum (FWHM) = 10 mm for HD-DOT and FWHM = 6 mm for fMRI]. Both DOT and fMRI-BOLD volumes were realigned to the representative adult template used at the Washington University Neuroimaging Laboratory (Smyser et al. 2010). This target is based on T_1-weighted images from 12 normal subjects and conforms to the Talairach atlas (Talairach and Tournoux 1988). After spatial normalization, all volumes were resampled to 3 mm isotropic voxels.

Seed-Based Correlation Analysis and Group Averaging

Seed regions were 6 mm radius spheres centered on ROIs selected by a neuroradiologist (J.S.S.) based on prior studies (Smyser et al. 2010; Zhang and Raichle 2010). Three pairs of seeds located in the visual (Vis), middle temporal visual area (MT), and auditory (A1) cortices (Supplementary Table 2) were chosen based on the DOT field of view (Fig. 3*a*). Time series were extracted for all seed regions and cross-correlated with all other voxels in the field of view to generate correlation maps using the standard Pearson product moment formula. Individual correlation maps for each modality were converted to a normal distribution by Fisher's z-transformation (Jenkins and Watts 1968) and averaged across subjects. Average maps were converted to Pearson's correlation coefficients for visualization purposes. A mean ROI-to-ROI correlation matrix including all seed regions was created.

Independent Component Analysis

The FastICA toolbox (Hyvarinen 1999) was employed as described previously (White et al. 2011). Eleven to 15 independent components (ICs) were extracted depending on the subject. From each data set, 3 ICs were chosen based on bilateral patterns that resembled those of the visual, middle temporal, and auditory RSNs. To generate group IC maps, each individual IC result was normalized to its maximum value and averaged together (Calhoun et al. 2001).

Results

Functional Connectivity Mapping

Seed-based correlation analysis, employing ROIs selected according to the subject-specific field of view, was used to create correlation maps for both DOT and fMRI data (Fig. 3*a*). DOT maps demonstrated strong interhemispheric correlation between homotopic counterparts for each of the 3 ROIs, indicating well-developed functional connectivity (Fig. 3*b* and Supplementary Fig. 2). Limited intrahemispheric connectivity was present. Subject-specific neonatal head modeling enabled direct spatial comparisons to nonconcurrent fcMRI data obtained in the same subjects. Qualitatively, there is strong spatial agreement in correlation maps between modalities for all hemodynamic contrasts at the individual level (Supplementary Fig. 3).

Using spatial normalization methods, individual results were mapped to a term neonatal template and mean correlation maps were created for each modality (Fig. 4). To visualize their spatial extent over the cortical surface, voxel maps were projected onto an average surface-based neonatal atlas (Van Essen et al. 2001). Following normalization, qualitative comparison of group

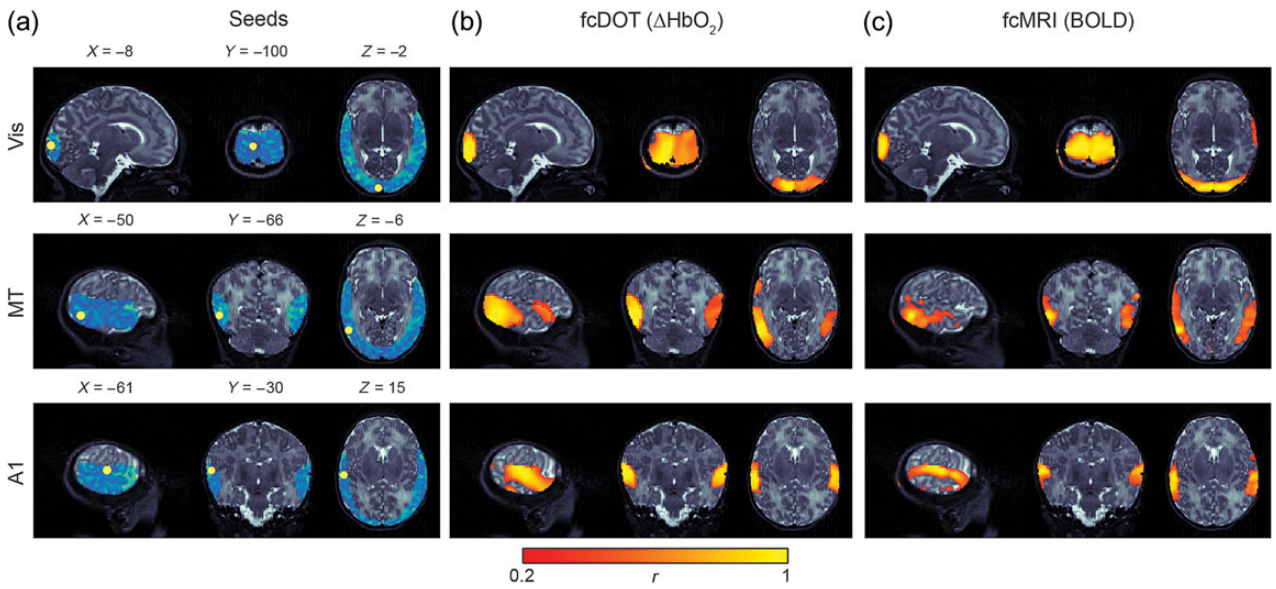

Figure 3. Single subject fcDOT and fcMRI comparisons. Resting-state functional connectivity maps obtained for a single infant. (*a*) ROI locations used in present analyses overlaid on subject-specific DOT field of view (blue). (*b*) Individual fcDOT correlation maps illustrating identified networks. (*c*) fcMRI results from comparable analysis. Note the high degree of spatial agreement between the fcDOT and fcMRI results. All results are overlaid onto sagittal, coronal, and axial slices of the infant's T_2-weighted MRI volume centered at each seed location. Color threshold $r > 0.2$ (Vis, visual; MT, middle temporal; A1, auditory).

mean correlation maps shows high spatial correspondence between fcDOT and fcMRI results (Fig. 4*a*). Similarities were also apparent in the ROI-to-ROI correlation matrices corresponding to all seed pairs generated for both modalities (Fig. 4*b*).

Quantitative comparison of the interhemispheric correlation between homotopic counterparts showed similar regional patterns across hemodynamic contrasts (Fig. 4*c*). Specifically, average homotopic interhemispheric correlation coefficients for ΔHbO_2, ΔHbR, ΔHbT, and BOLD, respectively, were 0.24, 0.21, 0.21, and 0.22 for MT seeds, 0.33, 0.33, 0.33, and 0.38 for auditory seeds, and 0.73, 0.57, 0.57, and 0.66 for visual seeds. Note that the regional differences in the interhemispheric correlation coefficients are strongly matched across fcDOT and fcMRI maps and within all of the fcDOT hemoglobin contrasts.

fcDOT and fcMRI Comparisons

fcDOT and fcMRI results were also interrogated on a voxel-by-voxel basis. The similarity of group results generated using each voxel as a seed location (as measured by the spatial correlation of 2 images) is relatively smooth and even, with decreasing values toward the edges of the field of view (Fig. 5). In particular, the spatial correlation values obtained for the seed regions were 0.57 and 0.58 for left and right MT seeds, 0.61 and 0.62 for left and right auditory seeds, and 0.68 and 0.64 for left and right visual seeds. Note that DOT and fMRI data were preprocessed using different smoothing kernels (FWHM = 10 mm for DOT; FWHM = 6 mm for fMRI), which may affect the similarity maps (or spatial correlation measures) obtained between modalities.

Independent Component Analysis

To evaluate results independent of ROI selection, we also analyzed fcDOT data using independent component analysis (ICA). This approach revealed ICs corresponding to visual, MT, and auditory RSNs for individual subjects. These ICs were also spatially normalized and averaged to generate group results for each network. Although quantitative comparisons between methods are limited by differences in data processing, qualitative comparisons between ICA and seed correlation analysis results reveal strong spatial agreement (Fig. 6).

Discussion

Summary of Findings

Our results demonstrate successful bedside mapping of multiple RSNs in healthy, full-term infants using fcDOT. While previous applications of this modality in hospitalized neonates had been limited to only mapping the occipital cortex (White et al. 2011), the present work extends these methods to include multiple functional regions and enables quantitative evaluation of regional patterns in functional connectivity. Furthermore, our results show strong qualitative and quantitative agreement with those obtained using fcMRI at both the individual and group levels, in contrast to findings from other optical imaging techniques. Finally, and perhaps most interestingly, the strength of the connectivity patterns measured using both fcDOT and fcMRI exhibits regional variability that is consistent with the typical trajectories observed in cortical maturation.

HD-DOT System Improvements and Advantages

The fcDOT methods applied in this investigation combine high-density arrays and superficial signal regression methods to separate cerebral signals from systemic artifacts (Gregg et al. 2010; Saager et al. 2011; Gagnon et al. 2012). While high-density arrays provide improved brain specificity and image resolution, they also introduce additional challenges related to cap ergonomics and management of fiber bundles. To ensure satisfactory optical coupling between fibers and scalp while providing sufficient support and comfort for extended scanning sessions in any clinical setting, a neonatal imaging cap was designed using a combination of silicone fiber feedthroughs and anatomically formed

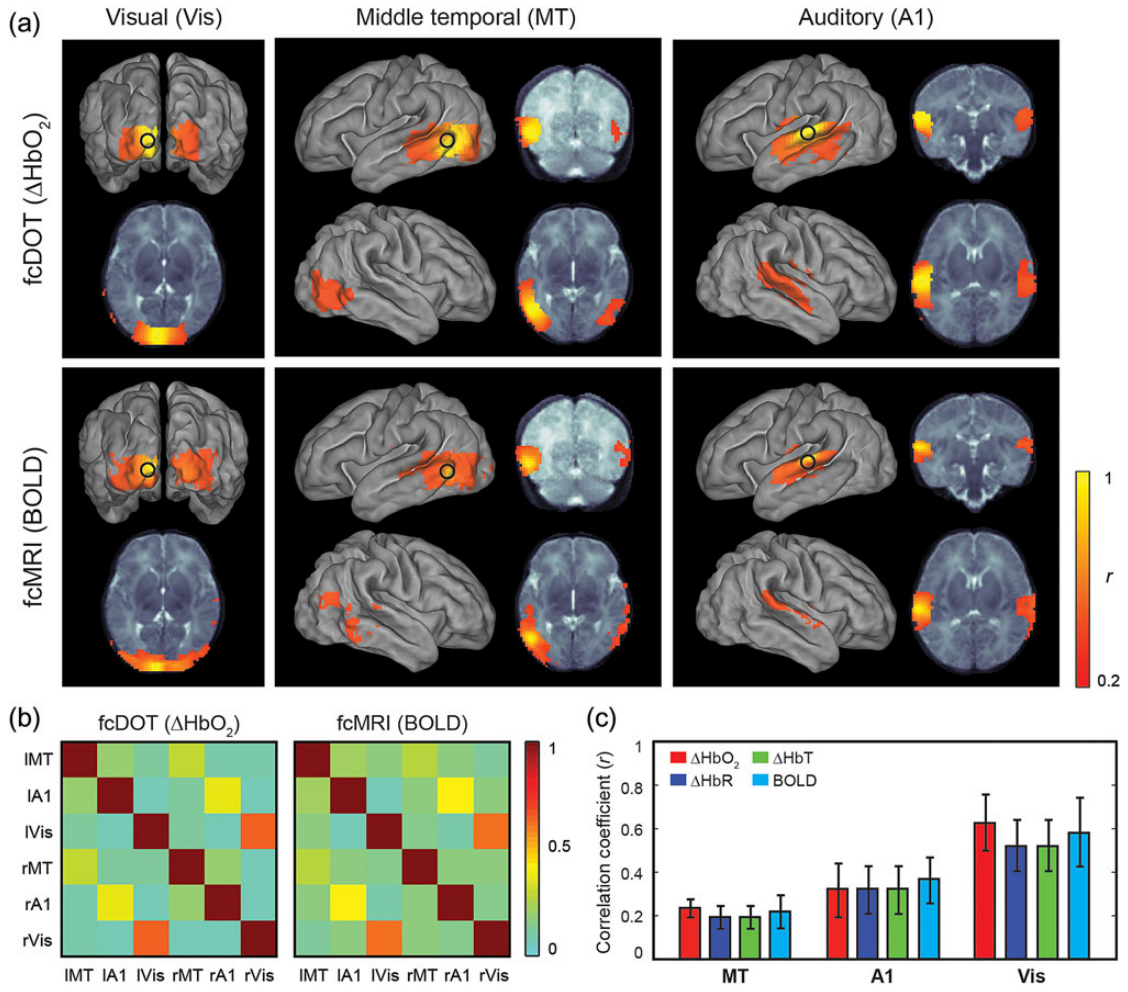

Figure 4. Group comparisons. (*a*) Average correlation maps for a group of 9 healthy, full-term infants. All maps are displayed on an average surface-based atlas of the neonatal cortex. (*b*) ROI-to-ROI correlation matrices for fcDOT (left) and fcMRI (right) group maps. Seeds are organized from left (l) to right (r). (*c*) Average interhemispheric correlations for each pair of seeds and contrasts (i.e., oxygenated hemoglobin, deoxygenated hemoglobin, total hemoglobin, and BOLD). Error bars denote standard error across subjects.

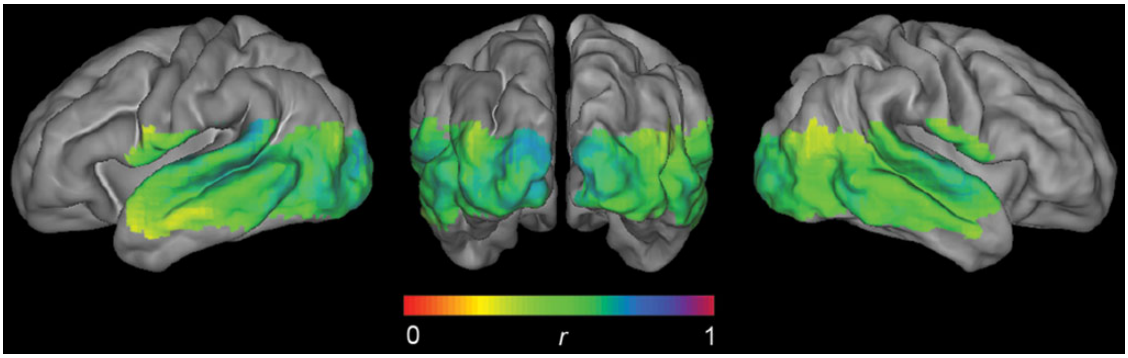

Figure 5. Voxelwise comparisons. Spatial correlations (Pearson's r) of correlation maps (ΔHbO_2 vs. BOLD) calculated for each possible seed located within the DOT field of view. The DOT field of view was defined as the intersection of the individual field of view (defined in the atlas space) corresponding to each subject.

plastic tiles integrated into a conformable neoprene headband (Fig. 1). In addition, to manage and optimize the cap fitting procedure, real-time visualizations of raw data quality were used to track and correct poor fiber-scalp coupling and subject motion issues. Motion artifacts are a frequent source of spurious correlations in functional neuroimaging investigations that require identification and censoring to ensure fidelity of results (Power et al. 2012).

Improvements in instrumentation and data quality motivate advancements in realistic forward light modeling. An early

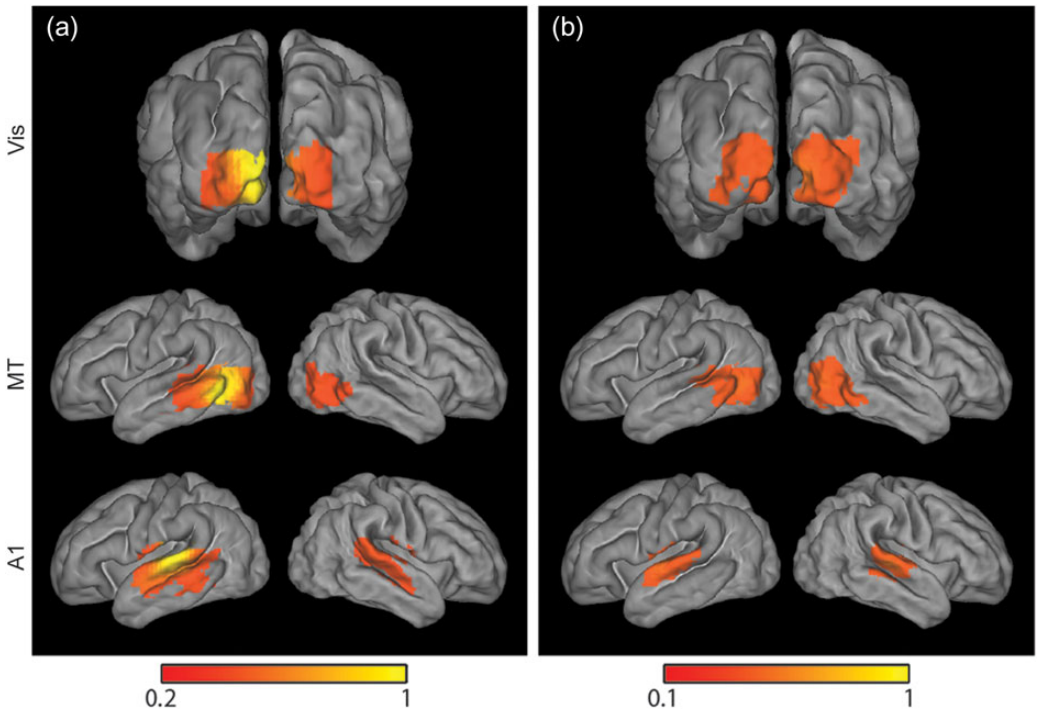

Figure 6. Seed-based versus ICA fcDOT group maps. Mean maps projected on the average surface-based neonatal atlas obtained using (*a*) seed-based correlation analysis and (*b*) ICA exhibit remarkably similar spatial patterns for 3 investigated resting-state networks.

example of infant DOT demonstrated the three-dimensional capabilities of finite element modeling (Hebden et al. 2002; Gibson et al. 2006). While a number of papers have reported sparse optical imaging in infants, the use of subject-specific, neonatal head models with anatomically derived interior tissue structures has been limited to simulation studies (Heiskala, Hiltunen, et al. 2009; Heiskala, Pollari, et al. 2009; Dehaes, Grant, et al. 2011; Dehaes et al. 2013). The lack of optical in vivo reports of fcDOT with anatomic head models is presumably due to the need for high-resolution neonatal MRI data and the limited availability of tools for automatic segmentation of neonatal brains. In this study, our neonatal head modeling pipeline enables accurate reconstruction of DOT data that is automatically coregistered with the infant's brain anatomy (Fig. 2). This approach facilitates spatial comparisons with other imaging modalities including fMRI (Figs 3 and 5), allows for spatial normalization and group averaging (Figs 4 and 6), and enables the use of standardized seed locations for functional connectivity analyses.

Comparison of fcDOT and fcMRI Results

There is remarkable qualitative and quantitative agreement between the functional connectivity measures obtained using fcDOT and fcMRI despite differences in spatial resolution. (fcDOT spatial resolution is ~10 mm, whereas fcMRI spatial resolution is ~6 mm.) Whereas both modalities enabled quantitative and qualitative assessment of investigated RSNs across all subjects with satisfactory data quality, HD-DOT provided these measures from testing performed at the bedside. The technical advances incorporated in the current system ensure this technology can be translated readily to any medical setting, from the normal newborn nursery to complex environments such as the neonatal intensive care unit (NICU). Thus, infants can undergo serial investigations of functional cerebral development throughout their nursery course, assessments not technically and logistically feasible for many neonatal clinical populations of interest using existing MRI technology.

In addition, due to the sensitivity to oxygenated and deoxygenated hemoglobin, NIRS techniques such as DOT can potentially provide information on regional changes of tissue oxygenation (StO_2) and oxygen extraction fraction in the infant brain (Franceschini et al. 2007). Recent efforts have demonstrated the feasibility and utility of measuring cerebral blood flow dynamics using laser speckle techniques (Durduran and Yodh 2014). When flow is combined with measures of OEF, the cerebral metabolic rate of oxygen consumption ($CMRO_2$) can be calculated (Culver et al. 2003; Durduran et al. 2004; Roche-Labarbe et al. 2010). These studies complement our studies of functional connectivity, particularly the work in infants which show that baseline hemodynamics change as a function of gestational and chronological age (Roche-Labarbe et al. 2012; Lin et al. 2013). This is particularly relevant to the study of infants born prematurely or with cerebral injury who might show atypical hemodynamic responses because their vasculature, and consequently their neurovascular coupling, is either not fully mature or injured (Colonnese et al. 2008; Arichi et al. 2012; Colonnese and Khazipov 2012; Kozberg et al. 2013).

Developmental Implications

Importantly, the interhemispheric correlation results for both fcDOT and fcMRI exhibit different strengths based on the region investigated (Vis > A1 > MT, where Vis, A1, and MT refer to the visual, auditory, and middle temporal visual cortical areas, respectively). These measures presumably reflect differential rates of RSN development, concordant with prior investigations in infants (Doria et al. 2010; Lagercrantz 2010; Smyser et al. 2010). It is assumed that the development of RSNs is dependent on

synchronous maturation of cortical gray and white matter, with identified patterns reflecting known spatial and temporal gradients in early structural cerebral development. Formation of RSNs is dependent on normative cortical development, beginning with subplate synaptogenesis and formation of thalamocortical connectivity. These procedures are programmatically followed by the establishment of cortical connections and proliferation of axons and glia. Synaptogenesis and overproduction of dendritic spines follow in a region- and cortical layer-specific manner, with increases in synaptic density and dendritic arborization leading to thickening of the cerebral cortex. Anatomic distance plays a key role in establishment of these early cortical connections. This cortical expansion is offset by programmed neuronal apoptosis and a protracted process of pruning and reorganization of weaker synapses and dendritic spines (Mrzljak et al. 1992; Petanjek et al. 2008, 2011; Lagercrantz 2010). Myelination, critical for enhancing propagation of action potentials, also begins during this period. This process also proceeds in an orderly manner, progressing outward from the central sulcus toward the poles, with posterior sites preceding frontotemporal locations. These structural processes are gradually shaped by emerging, spontaneous neuronal activity and external stimuli (Shatz 1996; Petanjek et al. 2011). Early development in the primary motor and sensory cortices (e.g., visual cortex) has been well described, while maturation in areas of association cortex, such as those located in the parietal or frontal lobes, occurs relatively slowly (Meyer 1961; Sidman and Rakic 1982; Lagercrantz 2010; Petanjek et al. 2011). The ranking of correlation coefficient magnitudes in this investigation is consistent with these patterns and suggests that fcDOT, similar to fcMRI, is sensitive to these neurodevelopmental changes (Smyser et al. 2016).

Relation to Previous Optical Studies of Functional Connectivity in Infants

A small number of prior studies have evaluated functional connectivity networks in healthy term (Homae et al. 2010) and preterm infants (Fuchino et al. 2013; Imai et al. 2014) using sparse optical arrays with larger SD separations (~2 cm). While the head coverage was relatively comprehensive, the connectivity analysis used the time series of single NIRS channels (i.e., SD pair measurements) rather than voxel data. In contrast to prior fcMRI investigations in neonates that demonstrated bilateral correlation between homotopic counterparts in both term- and prematurely born infants (Fransson et al. 2007, 2009; Lin et al. 2008; Doria et al. 2010; Smyser et al. 2010; Gao et al. 2011), these sparse optical studies reported only unilateral correlation patterns in newborn infants (i.e., no correlations were evident between homotopic regions). The reasons for the differences from fcMRI are not clear, though potentially partial volume effects and/or scalp contamination, both common in sparse optical array data, may be contributing factors. In contrast to the previous sparse optical studies, the congruence of these HD-DOT results with the neonatal fMRI neuroimaging literature suggests that HD-DOT imaging systems can provide image resolution sufficient for accurate and quantitative mapping of distributed functional networks.

Caveats and Limitations

The use of subject-specific structural MRIs validated the individualized DOT reconstructions relative to subject-matched fMRI maps. However, despite improved accuracy in forward head modeling, this approach is not sufficient for some portable applications (including serial fcDOT measurements) due to the need for subject-specific MRI. For infants without MRI, subject-specific head models can potentially be obtained by transforming atlas head models, as has been demonstrated for adults (Custo et al. 2010; Ferradal et al. 2014). The combination of atlas transformation techniques with aged-matched neonatal templates (Brigadoi et al. 2014) could provide realistic head models that integrate the detailed internal structure provided by the anatomical atlas and the subject's external head shape by means of a nonlinear warping procedure.

Owing to the poor image contrast of the very thin skull layer in the structural MRIs, head models with a single extracerebral layer that combined both skull and scalp optical properties were used. While identifying the skull layer is of critical importance in EEG forward modeling due to the electrical properties of bone, this is not the case in optical imaging applications where the neonatal optical properties of scalp and uncalcified skull are not significantly different (Heiskala, Pollari, et al. 2009; Dehaes, Kazemi, et al. 2011). Extensions of this work will consider generic head models with multiple extracerebral tissue layers, potentially derived from existing combined MRI (soft tissue) and CT (bone) data sets.

An obvious limitation of the current study is that the HD-DOT system used does not provide full head coverage of the infants. This limitation is faced by all current DOT systems. While healthy adults have been imaged with a larger (>1200) SD pair measurement system (Eggebrecht et al. 2014), for clinical imaging, the current channel count (>300) represents the state-of-the-art. For the purposes of establishing the regional correspondence between quantitative functional connection strengths, the field of view was sufficient. For more comprehensive mapping of the evolution of functional connectivity throughout development, an HD-DOT system with greater coverage will be required.

Conclusions

Bedside application of fcDOT enables accurate assessment of network-specific patterns of functional connectivity development in infants. Results for cortical networks investigated with fcDOT are similar to those obtained with fcMRI using qualitative and quantitative comparison approaches. Correlation coefficient magnitudes correspond to known rates of cortical maturation in healthy, term infants. These advances in acquisition and analysis methods enable successful and relatively faster collection of high quality fcDOT data in neonates in any medical setting, from the newborn nursery to the NICU. Establishing the relationship between fcDOT results, structural neuroimaging findings, and neurodevelopmental outcome measures may provide novel optical imaging biomarkers of brain injury and adverse neurodevelopmental outcomes that enable improvements in clinical care.

Supplementary Material

Supplementary material can be found at http://www.cercor.oxfordjournals.org/ online.

Funding

This work was supported in part by the National Institutes of Health (grant numbers K02 NS089852 [C.D.S.], UL1 TR000448 [C.D.S. and J.P.C.], R01 NS090874 [J.P.C.], R01 EB009233 [J.P.C], R21 EB007924 [J.P.C.], and KL2 TR000450 [S.M.L.]); Mallinckrodt Institute of Radiology (C.D.S. and J.P.C.); Fulbright Science and

Technology Ph.D. Award (S.L.F.), and Autism Speaks Meixner Postdoctoral Translational Research Fellowship (A.T.E.). The funding sources had no involvement in the study design, collection, analysis, interpretation of the data, writing of the paper, or decision to submit the paper for publication. J.P.C. and Washington University have financial interests in Cephalogics LLC based on a license of related optical imaging technology by the University to Cephalogics LLC.

Notes

We thank Martin Olevitch for his help with DOT acquisition software, Jim Alexopoulos for his assistance with ANTs software, and Jeanette Kenley for her valuable guidance with fcMRI analysis. We are also grateful to Anthony Barton and Karen Lukas for assisting with recruitment and clinical scanning. *Conflict of Interest*: J.P.C. and Washington University have financial interests in Cephalogics LLC based on a license of related optical imaging technology by the University to Cephalogics LLC.

References

Arichi T, Fagiolo G, Varela M, Melendez-Calderon A, Allievi A, Merchant N, Tusor N, Counsell SJ, Burdet E, Beckmann CF, et al. 2012. Development of BOLD signal hemodynamic responses in the human brain. Neuroimage. 63:663–673.

Avants BB, Tustison NJ, Wu J, Cook PA, Gee JC. 2011. An open source multivariate framework for n-tissue segmentation with evaluation on public data. Neuroinformatics. 9:381–400.

Boas DA, Chen K, Grebert D, Franceschini MA. 2004. Improving the diffuse optical imaging spatial resolution of the cerebral hemodynamic response to brain activation in humans. Opt Lett. 29:1506–1508.

Brigadoi S, Aljabar P, Kuklisova-Murgasova M, Arridge SR, Cooper RJ. 2014. A 4D neonatal head model for diffuse optical imaging of pre-term to term infants. Neuroimage. 100:385–394.

Calhoun VD, Adali T, McGinty VB, Pekar JJ, Watson TD, Pearlson GD. 2001. fMRI activation in a visual-perception task: network of areas detected using the general linear model and independent components analysis. Neuroimage. 14:1080–1088.

Colonnese M, Khazipov R. 2012. Spontaneous activity in developing sensory circuits: implications for resting state fMRI. Neuroimage. 62:2212–2221.

Colonnese MT, Phillips MA, Constantine-Paton M, Kaila K, Jasanoff A. 2008. Development of hemodynamic responses and functional connectivity in rat somatosensory cortex. Nat Neurosci. 11:72–79.

Culver JP, Durduran T, Furuya D, Cheung C, Greenberg JH, Yodh AG. 2003. Diffuse optical tomography of cerebral blood flow, oxygenation, and metabolism in rat during focal ischemia. J Cereb Blood Flow Metab. 23:911–924.

Custo A, Boas DA, Tsuzuki D, Dan I, Mesquita R, Fischl B, Grimson WE, Wells W III. 2010. Anatomical atlas-guided diffuse optical tomography of brain activation. Neuroimage. 49:561–567.

Dehaes M, Grant PE, Sliva DD, Roche-Labarbe N, Pienaar R, Boas DA, Franceschini MA, Selb J. 2011. Assessment of the frequency-domain multi-distance method to evaluate the brain optical properties: Monte Carlo simulations from neonate to adult. Biomed Opt Express. 2:552–567.

Dehaes M, Kazemi K, Pelegrini-Issac M, Grebe R, Benali H, Wallois F. 2011. Quantitative effect of the neonatal fontanel on synthetic near infrared spectroscopy measurements. Hum Brain Mapp. 34:878–889.

Dehaes M, Kazemi K, Pelegrini-Issac M, Grebe R, Benali H, Wallois F. 2013. Quantitative effect of the neonatal fontanel on synthetic near infrared spectroscopy measurements. Hum Brain Mapp. 34:878–889.

Dehghani H, Eames ME, Yalavarthy PK, Davis SC, Srinivasan S, Carpenter CM, Pogue BW, Paulsen KD. 2008. Near infrared optical tomography using NIRFAST: algorithm for numerical model and image reconstruction. Commun Numer Methods Eng. 25:711–732.

Doria V, Beckmann CF, Arichi T, Merchant N, Groppo M, Turkheimer FE, Counsell SJ, Murgasova M, Aljabar P, Nunes RG, et al. 2010. Emergence of resting state networks in the preterm human brain. Proc Natl Acad Sci USA. 107:20015–20020.

Dubois J, Dehaene-Lambertz G, Kulikova S, Poupon C, Huppi PS, Hertz-Pannier L. 2014. The early development of brain white matter: a review of imaging studies in fetuses, newborns and infants. Neuroscience. 276C:48–71.

Durduran T, Yodh AG. 2014. Diffuse correlation spectroscopy for non-invasive, micro-vascular cerebral blood flow measurement. Neuroimage. 85(Pt 1):51–63.

Durduran T, Yu G, Burnett MG, Detre JA, Greenberg JH, Wang J, Zhou C, Yodh AG. 2004. Diffuse optical measurement of blood flow, blood oxygenation, and metabolism in a human brain during sensorimotor cortex activation. Opt Lett. 29: 1766–1768.

Eggebrecht AT, Ferradal SL, Robichaux-Viehoever A, Hassanpour MS, Dehghani H, Snyder AZ, Hershey T, Culver JP. 2014. Mapping distributed brain function and networks with diffuse optical tomography. Nat Photonics. 8:448–454.

Eggebrecht AT, White BR, Ferradal SL, Chen C, Zhan Y, Snyder AZ, Dehghani H, Culver JP. 2012. A quantitative spatial comparison of high-density diffuse optical tomography and fMRI cortical mapping. Neuroimage. 61:1120–1128.

Ferradal SL, Eggebrecht AT, Hassanpour M, Snyder AZ, Culver JP. 2014. Atlas-based head modeling and spatial normalization for high-density diffuse optical tomography: in vivo validation against fMRI. Neuroimage. 85(Pt 1):117–126.

Franceschini MA, Thaker S, Themelis G, Krishnamoorthy KK, Bortfeld H, Diamond SG, Boas DA, Arvin K, Grant PE. 2007. Assessment of infant brain development with frequency-domain near-infrared spectroscopy. Pediatr Res. 61:546–551.

Fransson P, Skiöld B, Engström M, Hallberg B, Mosskin M, Åden U, Lagercrantz H, Blennow M. 2009. Spontaneous brain activity in the newborn brain during natural sleep–an fMRI study in infants born at full term. Pediatr Res. 66:301–305.

Fransson P, Skiold B, Horsch S, Nordell A, Blennow M, Lagercrantz H, Aden U. 2007. Resting-state networks in the infant brain. Proc Natl Acad Sci USA. 104:15531–15536.

Fuchino Y, Naoi N, Shibata M, Niwa F, Kawai M, Konishi Y, Okanoya K, Myowa-Yamakoshi M. 2013. Effects of preterm birth on intrinsic fluctuations in neonatal cerebral activity examined using optical imaging. PLoS ONE. 8:e67432.

Gagnon L, Cooper RJ, Yucel MA, Perdue KL, Greve DN, Boas DA. 2012. Short separation channel location impacts the performance of short channel regression in NIRS. Neuroimage. 59: 2518–2528.

Gao W, Gilmore JH, Giovanello KS, Smith JK, Shen D, Zhu H, Lin W. 2011. Temporal and spatial evolution of brain network topology during the first two years of life. PLoS ONE. 6:e25278.

Gibson AP, Austin T, Everdell NL, Schweiger M, Arridge SR, Meek JH, Wyatt JS, Delpy DT, Hebden JC. 2006. Three-dimensional whole-head optical tomography of passive

motor evoked responses in the neonate. Neuroimage. 30: 521–528.

Glass HC, Bonifacio SL, Peloquin S, Shimotake T, Sehring S, Sun Y, Sullivan J, Rogers E, Barkovich AJ, Rowitch D, et al. 2010. Neurocritical care for neonates. Neurocrit Care. 12:421–429.

Gregg NM, White BR, Zeff BW, Berger AJ, Culver JP. 2010. Brain specificity of tissue optical imaging: improvements from superficial signal regression and tomography. Front Neuroenerget. 2:1–8.

Habermehl C, Holtze S, Steinbrink J, Koch SP, Obrig H, Mehnert J, Schmitz CH. 2012. Somatosensory activation of two fingers can be discriminated with ultrahigh-density diffuse optical tomography. Neuroimage. 59:3201–3211.

Hebden JC, Gibson A, Yusof RM, Everdell N, Hillman EM, Delpy DT, Arridge SR, Austin T, Meek JH, Wyatt JS. 2002. Three-dimensional optical tomography of the premature infant brain. Phys Med Biol. 47:4155–4166.

Heiskala J, Hiltunen P, Nissila I. 2009. Significance of background optical properties, time-resolved information and optode arrangement in diffuse optical imaging of term neonates. Phys Med Biol. 54:535–554.

Heiskala J, Pollari M, Metsaranta M, Grant PE, Nissila I. 2009. Probabilistic atlas can improve reconstruction from optical imaging of the neonatal brain. Opt Express. 17:14977–14992.

Hill J, Inder T, Neil J, Dierker D, Harwell J, Van Essen D. 2010. Similar patterns of cortical expansion during human development and evolution. Proc Natl Acad Sci USA. 107:13135–13140.

Homae F, Watanabe H, Otobe T, Nakano T, Go T, Konishi Y, Taga G. 2010. Developmend of global cortical networks in early infancy. J Neurosci. 30:4877–4882.

Hyvarinen A. 1999. Fast and robust fixed-point algorithms for independent component analysis. IEEE Trans Neural Netw. 10:626–634.

Imai M, Watanabe H, Yasui K, Kimura Y, Shitara Y, Tsuchida S, Takahashi N, Taga G. 2014. Functional connectivity of the cortex of term and preterm infants and infants with Down's syndrome. Neuroimage. 85(Pt 1):272–278.

Jenkins GM, Watts DG. 1968. Spectral analysis and its applications. San Francisco: Holden-Day.

Jermyn M, Ghadyani H, Mastanduno MA, Turner W, Davis SC, Dehghani H, Pogue BW. 2013. Fast segmentation and high-quality three-dimensional volume mesh creation from medical images for diffuse optical tomography. J Biomed Opt. 18:86007.

Jernigan TL, Baare WF, Stiles J, Madsen KS. 2011. Postnatal brain development: structural imaging of dynamic neurodevelopmental processes. Prog Brain Res. 189:77–92.

Kozberg MG, Chen BR, DeLeo SE, Bouchard MB, Hillman EM. 2013. Resolving the transition from negative to positive blood oxygen level-dependent responses in the developing brain. Proc Natl Acad Sci USA. 110:4380–4385.

Lagercrantz H. 2010. The newborn brain neuroscience and clinical applications. 2nd ed. New York: Cambridge University Press.

Lin PY, Roche-Labarbe N, Dehaes M, Fenoglio A, Grant PE, Franceschini MA. 2013. Regional and hemispheric asymmetries of cerebral hemodynamic and oxygen metabolism in newborns. Cereb Cortex. 23:339–348.

Lin W, Zhu Q, Gao W, Chen Y, Toh C-H, Styner M, Gerig G, Smith JK, Biswal B, Gilmore JH. 2008. Functional connectivity MR imaging reveals cortical functional connectivity in the developing brain. Am J Neuroradiol. 29:1883–1889.

Mathur AM, Neil JJ, McKinstry RC, Inder TE. 2008. Transport, monitoring, and successful brain MR imaging in unsedated neonates. Pediatr Radiol. 38:260–264.

Meyer A. 1961. A note on the postnatal development of the human cerebral cortex. Cereb Palsy Bull. 3:263–268.

Mrzljak L, Uylings HB, Kostovic I, van Eden CG. 1992. Prenatal development of neurons in the human prefrontal cortex. II. A quantitative Golgi study. J Comp Neurol. 316:485–496.

Petanjek Z, Judas M, Kostovic I, Uylings HB. 2008. Lifespan alterations of basal dendritic trees of pyramidal neurons in the human prefrontal cortex: a layer-specific pattern. Cereb Cortex. 18:915–929.

Petanjek Z, Judas M, Simic G, Rasin MR, Uylings HB, Rakic P, Kostovic I. 2011. Extraordinary neoteny of synaptic spines in the human prefrontal cortex. Proc Natl Acad Sci USA. 108:13281–13286.

Power JD, Barnes KA, Snyder AZ, Schlaggar BL, Petersen SE. 2012. Spurious but systematic correlations in functional connectivity MRI networks arise from subject motion. Neuroimage. 59:2142–2154.

Roche-Labarbe N, Carp SA, Surova A, Patel M, Boas DA, Grant PE, Franceschini MA. 2010. Noninvasive optical measures of CBV, StO(2), CBF index, and rCMRO(2) in human premature neonates' brains in the first six weeks of life. Hum Brain Mapp. 31:341–352.

Roche-Labarbe N, Fenoglio A, Aggarwal A, Dehaes M, Carp SA, Franceschini MA, Grant PE. 2012. Near-infrared spectroscopy assessment of cerebral oxygen metabolism in the developing premature brain. J Cereb Blood Flow Metab. 32:481–488.

Saager RB, Telleri NL, Berger AJ. 2011. Two-detector corrected near infrared spectroscopy (C-NIRS) detects hemodynamic activation responses more robustly than single-detector NIRS. Neuroimage. 55:1679–1685.

Shatz CJ. 1996. Emergence of order in visual system development. Proc Natl Acad Sci USA. 93:602–608.

Sidman RL, Rakic P. 1982. Development of the human central nervous system. In: Histology and histopathology of the nervous system. Springfield (IL): Charles C. Thomas.

Smyser CD, Inder TE, Shimony JS, Hill JE, Degnan AJ, Snyder AZ, Neil JJ. 2010. Longitudinal analysis of neural network development in preterm infants. Cereb Cortex. 20:2852–2862.

Smyser CD, Snyder AZ, Shimony JS, Mitra A, Inder TE, Neil JJ. 2016. Resting-state network complexity and magnitude are reduced in prematurely born infants. Cereb Cortex. 26:322–333.

Talairach J, Tournoux P. 1988. Co-planar stereotaxic atlas of the human brain: 3-D proportional system: an approach to cerebral imaging. New York: Thieme Classics.

Tau GZ, Peterson BS. 2010. Normal development of brain circuits. Neuropsychopharmacology. 35:147–168.

Van Essen DC, Drury HA, Dickson J, Harwell J, Hanlon D, Anderson CH. 2001. An integrated software suite for surface-based analyses of cerebral cortex. J Am Med Inform Assoc. 8:443–459.

White BR, Liao SM, Ferradal SL, Inder TE, Culver JP. 2011. Bedside optical imaging of occipital resting-state functional connectivity in neonates. Neuroimage. 59:2529–2538.

Wray S, Cope M, Delpy DT, Wyatt JS, Reynolds EO. 1988. Characterization of the near infrared absorption spectra of cytochrome aa3 and haemoglobin for the non-invasive monitoring of cerebral oxygenation. Biochim Biophys Acta. 933:184–192.

Zeff BW, White BR, Dehghani H, Schlaggar BL, Culver JP. 2007. Retinotopic mapping of adult human visual cortex with high-density diffuse optical tomography. Proc Natl Acad Sci USA. 104:12169–12174.

Zhang D, Raichle ME. 2010. Disease and the brain's dark energy. Nat Rev Neurol. 6:15–28.